Article | Received 29 July 2024; Accepted 31 October 2024; Published 19 November 2024
https://doi.org/10.55092/asymmetry20240006

Pattern formation in a model of inflammation

Wissam El Hajj[1], Maxim Kuznetsov[2] and Vitaly Volpert[1,3,*]

[1] Universite Claude Bernard Lyon 1, CNRS, Ecole Centrale de Lyon, INSA Lyon, Université Jean Monnet, ICJ UMR5208, 69622 Villeurbanne, France

[2] Department of Computational and Quantitative Medicine, Division of Mathematical Oncology, City of Hope, Duarte, CA 91010, USA

[3] Peoples' Friendship University of Russia (RUDN University), 6 Miklukho-Maklaya St, Moscow 117198, Russian Federation

* Correspondence author; E-mail: volpert@math.univ-lyon1.fr.

Abstract: Inflammation is the body's response to infection, injury, or other stimuli. Acute inflammation is a crucial component of the immune system's defense, aimed at eliminating infected or damaged cells and halting disease progression. A subtle interaction between pro- and anti-inflammatory processes determines its progression to inflammation resolution or to chronic inflammation. In this study, we propose a generic model of inflammation through a system of reaction-diffusion equations involving various inflammatory and anti-inflammatory cells and cytokines. We investigate the formation of patterns, determined by the emergence of Turing structures, through linear stability analysis and numerical simulations. These theoretical findings are further supported by observations of similar patterns in skin diseases.

Keywords: inflammation; modelling; pattern formation; Turing structures

1. Introduction

1.1. Biological background

Inflammation is an important mechanism participating in the immune response to harmful stimuli. Many cellular and molecular pathways are activated during the inflammatory process [1]. Inflammation has some disease-specific features, but the mechanism of the immune response is generic [2]. It starts with the identification of primary stimuli by cell surface patterns recognition receptors (PRRs). PRRs are proteins whose role is to sense a specific type of dangerous stimuli such as DAMPs (Damage-associated molecular pattern molecules) or PAMPs (Pathogen-associated molecular pattern molecules). The recognition process leads to the activation of intra-cellular signalling pathways such as NF-κB, MAPK and JAK-STAT pathways which causes gene transcription activation on the cellular level. Therefore, numerous inflammatory agents such as inflammatory cytokines and chemokines are released [3]. Then,

immune cells migrate from the bloodstream to the region of inflammation [4]. After the set-up of the immune response, inflammatory agents are mobilized in order to restore homeostasis and to resolve inflammation. An effective anti-inflammatory process is needed to promote the reduction of inflammation [5]. If sensors of blood-circulating monocytes do not detect stimuli, monocytes are not recruited to the site of inflammation. Conversely, in cases of uncontrolled inflammation, acute inflammation fails to stop tissue damage, leading to chronic inflammatory conditions. This imbalance contributes to the progression of various inflammatory diseases such as cancer [6], atherosclerosis [7] or skin diseases [8].

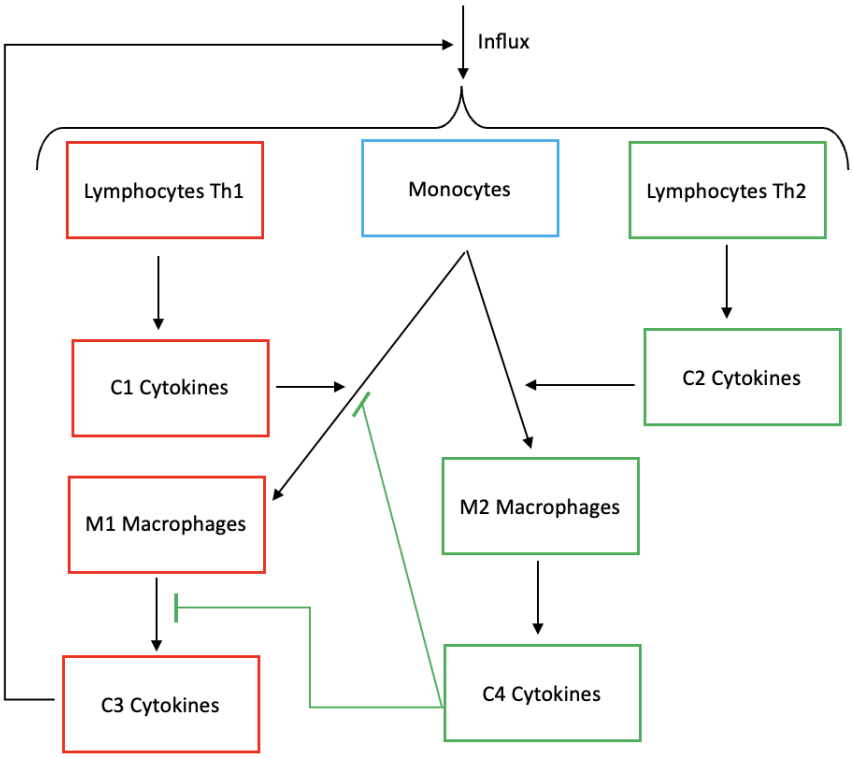

Figure 1. Scheme depicting the biological phenomena of inflammation including Th1-Th2 lymphocytes, monocytes, M1-M2 macrophages, C1-C2 cytokines and C3-C4 cytokines. Inflammatory cytokines C3 (IL-6, IL-12, TNF-α) induce the influx of lymphocytes and monocytes. Th1 produce C1 cytokines (IL-1β, IFN-γ) and promote differentiation of monocytes into M1 macrophages. Similarly, Th2 produce C2 cytokines (IL-4, IL-13) and promote differentiation of monocytes into M2 macrophages. Classically activated macrophages (M1) and alternatively activated macrophages (M2) produce respectively pro-inflammatory C3 and anti-inflammatory cytokines C4 (IL-10, TGF-β). C4 anti-inflammatory cytokines inhibit the production of pro-inflammatory cytokines and the differentiation of monocytes into M1 macrophages.

In the process of immune response, immune cells perform significant and crucial functions. A major step in the immune response is the recruitment of immune cells to the area of inflammation such as T cells, lymphocytes and monocytes. T cells are a type of leukocytes that differentiate into several subtypes such as T-helper cells Th1 and Th2 that regulate the maturation of monocytes into macrophages [9]. Th1 cells are considered pro-inflammatory because they secrete INFγ [10] to activate M1 type macrophages as shown in Figure 1. Classically activated macrophages (M1) produce pro-inflammatory cytokines, promote elimination of affected tissue cells, inhibits cell proliferation and causes the recruitment of additional immune cells to the

inflammation site. Conversely, alternatively activated macrophages (M2 type) are induced by Il-4 and IL-13 produced by Th2 cells [11]. Unlike M1 macrophages, M2 macrophages promote cell repair and cells proliferation [12]. Similarly to macrophages, inflammatory cytokines can be categorized into two types: pro-inflammatory and anti-inflammatory. Pro-inflammatory cytokines, such as TNF-α, IL-12, and IL-6, are produced to enhance inflammation. In contrast, IL-10, IL-4 and TGF-β are anti-inflammatory cytokines produced to down-regulate inflammation [13] by inhibiting the production of pro-inflammatory cytokines [14, 15].

Inflammation plays a major role in skin diseases since it is essential for defending against infection and injury but can also lead to chronic skin conditions when uncontrolled. For example, acne results from inflammation of hair follicles and sebaceous glands [16]. Another important example of skin diseases is eczema (atopic dermatitis) which touches one out of four school-aged children [17] and causes the skin to become dry and itchy due to an overactive immune system in response to allergens or irritants. The emergence of such diseases starts by the disruption of the epidermal barrier of the human skin [18] and can be due to several risk factors such as genetics, obesity and alcohol consumption [19, 20]. The effect of such disruptions leads to genetic mutations and impairment of the epidermal barrier functions [21] that affect the functioning, polarization of cells and the secretion of cytokines [19]. As a result, skin inflammation can arise depending on a dysfunctional immune response and an excessive production of pro-inflammatory cytokines by macrophages and dendritic cells [22, 23]. Atopic dermatitis is highlighted by an abnormal immune response including enhanced type 2 inflammation correlated by overexpression of inflammatory cytokines (IL-4 and IL-13). Type 2 inflammatory cytokines inhibit the expression of epidermal proteins (FLG) and promote the itch-scratch cycle by activating neurons [24]. Hence, a dysfunction in the inflammatory processes induces loss of epidermal integrity, chronic inflammation of the skin, and increased sensitivity to infections. As a result, many symptoms appear on the skin such as red papules and plaques. Several treatment approaches are considered in order to suppress the inflammatory process particularly the production of pro-inflammatory cytokines. For example, SOCS proteins regulates the signaling of pro-inflammatory cytokines through the modulation of the JAK/STAT pathway [23].

1.2. Modelling of inflammation

Theoretical modelling of inflammation is tackled by different approaches particularly the study of inflammation initiation due to respiratory infections [25]. Authors present a system of nonlinear ordinary differential equations to study the interactions between macrophages, pro-inflammatory, bacteria and anti-inflammatory cytokines. The study shows that an inflammatory state can set-up depending on the model parameters. According to [25], anti-inflammatory cytokines helps to reduce the intensity of inflammation. Mathematical modelling is a valuable tool to understand the interplay between pro-inflammatory and anti-inflammatory signaling [26]. The study presents a mathematical model to describe the interplay between Tumor Necrosis Factor (TNF) and IL-10 inflammatory cytokines in monocytes. Based on experimental data collection, authors show the role of IL-10 early feedback in switching the inflammation. Several studies describes the propagation of inflammation in tissue as a

reaction-diffusion wave [27–29], in particular, in atherosclerosis models. The interplay between macrophages, pro-inflammatory cytokines and oxidized low-density lipoproteins (ox-LDL) triggers the set-up of inflammation. For example, authors in [29] study the early stages of atherosclerosis through a mathematical model based on partial differential equations of reaction-diffusion type. They examine the effect of anti-inflammatory processes on the disease progression, finding that they can lead to plaque regression. Several studies have focused on the effect of some key-players in order to understand the development of some diseases such as the role of endothelial permeability in atherosclerosis [30] and the role of immune response in colorectal cancer [31]. For example, authors in [31] propose a model to study colorectal cancer growth and its response to chemo-immunotherapy. It shows how the immune system, namely the pro-inflammatory cytokine IL-2, interacts with chemotherapy.

Some studies have tackled the role of mathematical modeling in the understanding and describing the dynamics of skin diseases [32–35]. For example, authors in [32] emphasize the importance of integrating experimental data and mathematical modeling to improve skin research. Moreover, they suggest that the incorporation of mathematical studies can lead to more effective and personalized treatments in the future via drug optimization. Authors in [33] developed mathematical models based on partial and ordinary differential equations to study the role of chronic inflammation in the epidermis. They suggest potential therapeutic strategies to manage chronic inflammation by targeting specific components of the immune response in the field of skin biology. Authors in [34] propose a model to study the role of immune cell in inflammation with a focus on psoriasis (a chronic skin disease). By simulating cytokines production patterns, the model predicts that small alterations in inflammatory cytokines production can lead to the appearance of pathologic inflammatory levels. This model highlights that the feedback loop interaction between immune cells and cytokines can lead to spatial patterns. An indicator of such pattern formation is a high concentration of cytokines.

1.3. Pattern formation

Spatiotemporal patterns formation is widely manifested in various systems far from the thermodynamic equilibrium and exchanging matter and energy with the environment [36]. A. Turing suggested that organ formation in living organisms occurs due to the instability of a spatially homogeneous state in a system of interacting chemicals (morphogens) distributed over the growing embryo [37]. The non-homogeneous distribution of the concentrations of these chemicals influences the behavior of cells leading to their differentiation and organ formation. There are some experimental confirmations of this mechanism, in particular, for the growth of birds' feathers [38], for the branching pattern of lungs [39], the formation of fingers [40], and the left-right asymmetry of body organs [41]. Authors in [42] study the development of the mammalian lung through branching morphogenesis. They showed the role of Turing instability and that the branching patterns are driven by high local morphogen concentration. Predicting the form of the patterns has fascinated numerous researchers. In fact, several mathematical techniques are implemented for such sake, such as the weakly nonlinear analysis [43–46]. For example, authors in [43] study pattern formation in a two-dimensional domain for a reaction-diffusion system

with nonlinear diffusion terms and competitive Lotka-Volterra kinetics. They show, using a weakly nonlinear analysis, that the amplitude of equations can be derived to characterize pattern dynamics. Moreover, they describe that the cross-diffusion is a essential in the formation of several spatial patterns, such as rolls and hexagons. Authors in [46] examine the shape and stability of axisymmetric stationary patterns in a reaction-diffusion-chemotaxis model. They simulate skin lesions arising in acute inflammation by focusing on the interaction between immune cell chemotaxis and cytokines concentration. The weakly nonlinear analysis further clarifies how pro- and anti-inflammatory factors determine lesion shape since simulations obtained align with clinical observations of skin rashes. Turing instability has been also identified in many non-biological systems [47–50].

The conditions of the emergence of dissipative structures in a two-component systems can be formulated in terms of short-range activation and long-range inhibition, since one of the variables, referred to as a self-activator, should up-regulate its own production at the uniform stationary state, and another variable should be a self-inhibitor, acting in the opposite way. Moreover, the diffusion coefficient of the self-inhibitor should be sufficiently higher than that of the self-activator. It is worth noting, that although this is the general concept for emergence of Turing patterns in the systems with greater number of variables as well [51, 52], another possibilities for Turing patterns formation exist in multi-component systems, that can bypass the requirement of short-range activator and long-range inhibitor [53]. However, this requirement is strictly necessary for two-component systems.

Pattern formation in biomedical models can be determined by different mechanisms. As such, the interaction of inflammation and chemotaxis can result in formation of fatty streaks in atherosclerosis [54]. Authors in [55] propose that pattern formation can happen through combining chemotaxis and dynamics of anti-inflammatory cytokines. They suggest that spatial patterns form as immune cells move towards higher concentrations of chemo-attractants with a slow-inhibition anti-inflammatory process. Turing instability was suggested as the mechanism of pattern formation in Crohn's disease [56]. Authors proposed a reaction-diffusion system modelling the immune response that triggers inflammatory bowel diseases. They showed that under some conditions, an activator-inhibitor dynamic can be reproduced leading to the appearance of Turing-type instabilities. In this work we study pattern formation in a generic model of inflammation with short-range activation (inflammation) and long-range inhibition (anti-inflammation) mechanism and discuss it in the context of skin diseases.

2. Model of immune response and inflammation

Inflammation as a part of the immune response includes several steps common for different diseases. They are based on the interaction of different immune cells (monocytes, macrophages, lymphocytes) and cytokines as described in Figure 1, in a part of the skin considered as an open bounded domain $\Omega \subset \mathbf{R^2}$. We formulate in this section a generic model of inflammation and reduce it to a simpler two-equation model in order to perform its stability analysis. All parameters of the model are taken to be non-negative.

2.1. Generic model of inflammation

We formulate the model of inflammation for the concentrations of pro- and anti-inflammatory monocytes (N_1, N_2), macrophages (M_1, M_2), lymphocytes (T_1, T_2), cytokines produced by lymphocytes (C_1, C_2) and cytokines produced by macrophages (C_3, C_4). We employ a similar technique as [29] for the construction of the model. All parameters are taken to be non-negative. Equations for pro-inflammatory monocytes N_1 and anti-inflammatory monocytes N_2 are considered in the following form:

$$\frac{dN_1}{dt} = \lambda_{PN_1}\frac{C_3}{k_{1P}+k_{2P}C_3}N_1^0 - \lambda_{C_1N_1}\frac{C_1}{k_{C_1}+C_1+k_4C_4}N_1 - d_{N_1}N_1, \tag{2.1}$$

$$\frac{dN_2}{dt} = \lambda_{PN_2}\frac{C_3}{k_{1P}+k_{2P}C_3}N_2^0 - \lambda_{C_2N_2}\frac{C_2}{k_{C_2}+C_2}N_2 - d_{N_2}N_2. \tag{2.2}$$

The constants λ_{PN_1} and λ_{PN_2} characterize the rate of monocytes influx to the inflammation site, N_1^0 and N_2^0 are the densities of the corresponding monocytes in blood, d_{N_1} and d_{N_2} are the death rates of N_1 and N_2 monocytes. Cell influx depends on the concentration of inflammatory cytokines C_3 with saturation [57]. Thus, the first terms in the right-hand sides of these equations represent the influx of monocytes from the blood [4], the second terms describe the differentiation of monocytes into macrophages [58–60], and the third terms correspond to the death of monocytes.

Next, in the equations for pro-inflammatory macrophages M_1 and anti-inflammatory macrophages M_2

$$\frac{dM_1}{dt} = \lambda_{C_1N_1}\frac{C_1}{k_{C_1}+C_1+k_4C_4}N_1 - d_{M_1}M_1, \tag{2.3}$$

$$\frac{dM_2}{dt} = \lambda_{C_2N_2}\frac{C_2}{k_{N_2}+C_2}N_2 - d_{M_2}M_2, \tag{2.4}$$

the first terms in the right-hand sides characterize the differentiation of monocytes into macrophages [58–60] and the last terms d_{M_1} and d_{M_2} are the death rates of M_1 and M_2 macrophages, respectively.

Equations for T-helper cells T_1 and T_2 are as follows:

$$\frac{dT_1}{dt} = \lambda_{PT_1}\frac{C_3}{k_{1P}+k_{2P}C_3}T_1^0 - d_{T_1}T_1, \tag{2.5}$$

$$\frac{dT_2}{dt} = \lambda_{PT_2}\frac{C_3}{k_{1P}+k_{2P}C_3}T_2^0 - d_{T_2}T_2. \tag{2.6}$$

They model the influx of T-cells from the blood (similar to monocytes) [61] and death of T-cells. Here λ_{PT_1} and λ_{PT_2} are the rates of cell penetration, T_1^0 and T_2^0 are the densities of T_1 and T_2 cells in blood, d_{T_1} and d_{T_2} are the death rates of T_1 and T_2 cells.

Equations for cytokines C_1 produced by T_1 cells (IFN-γ, IL-1β) and C_2 (IL-4, IL-13) produced by T_2 cells

$$\frac{dC_1}{dt} = \lambda_{C_1}T_1 - k_{C_1N_1}C_1N_1 - d_{C_1}C_1, \tag{2.7}$$

$$\frac{dC_2}{dt} = \lambda_{C_2} T_2 - k_{C_2N_2} C_2 N_2 - d_{C_2} C_2 \tag{2.8}$$

describe production of cytokines C_1 and C_2 by T-lymphocytes with the rates λ_{C_1} and λ_{C_2}. They promote the differentiation of N_1 and N_2 monocytes into M_1 and M_2 macrophages with rate constants $k_{C_1N_1}$ and $k_{C_2N_2}$ and consumed (internalized) due to this interaction [59]. The third terms correspond to the degradation of cytokines with the rate constants d_{C_1} and d_{C_2}.

Equation for pro-inflammatory cytokines (IL-6, IL-12 and TNF-α) produced by macrophages:

$$\frac{dC_3}{dt} = \lambda_{C_4M_1} \frac{1}{k_{C_4} + C_4} M_1 - d_{C_3} C_3. \tag{2.9}$$

Macrophages M_1 produce pro-inflammatory cytokines C_3 with the rate constant $\lambda_{C_4M_1}$ activating endothelial cells [59]. The second term corresponds to the degradation of cytokines with the rate d_{C_3}. Anti-inflammatory cytocines C_4 downregulate C_3 production. Equation for anti-inflammatory cytokines (IL-10 and TGF-β) produced by macrophages:

$$\frac{dC_4}{dt} = \lambda_{C_4} M_2 - d_{C_4} C_4. \tag{2.10}$$

M_2 macrophages produce anti-inflammatory cytokines C_4 with rate λ_{C_4} [58, 59, 62]. They prevent cell penetration in the tissue. The second term corresponds to the degradation of these cytokines.

Positivity, boundedness and existence of solutions

In this section, we study the existence, uniqueness, positivity and boundedness of the solution for the system of equations (2.1)-(2.10).

Lemma 2.1. *For any non-negative initial condition* $(N_1(0), N_2(0), M_1(0), M_2(0), T_1(0), T_2(0), C_1(0), C_2(0), C_3(0), C_4(0))$*, the system (2.1)-(2.10) has a unique global solution which is bounded.*

Proof. Existence and uniqueness of a local solution are straightforward from the Cauchy–Lipschitz theorem for ordinary differential equations. For the positivity of solutions, consider the vector field $F = (f_1, ..., f_{10})$ for $x = (x_1, ..., x_{10}) \in \mathbf{R^{10}}$ given by

$$\begin{cases}
f_1(x) = \lambda_{PN_1} \frac{x_9}{k_{1P} + k_{2P} x_9} N_1^0 - \lambda_{C_1N_1} \frac{x_7}{k_{C_1} + x_7 + k_4 x_{10}} x_1 - d_{N_1} x_1, \\
f_2(x) = \lambda_{PN_2} \frac{x_9}{k_{1P} + k_{2P} x_9} N_2^0 - \lambda_{C_2N_2} \frac{x_8}{k_{C_2} + x_8} x_2 - d_{N_2} x_2, \\
f_3(x) = \lambda_{C_1N_1} \frac{x_7}{k_{C_1} + x_7 + k_4 x_{10}} x_1 - d_{M_1} x_3, \\
f_4(x) = \lambda_{C_2N_2} \frac{x_8}{k_{N_2} + x_8} x_2 - d_{M_2} x_4, \\
f_5(x) = \lambda_{PT_1} \frac{x_9}{k_{1P} + k_{2P} x_9} T_1^0 - d_{T_1} x_5, \\
f_6(x) = \lambda_{PT_2} \frac{x_9}{k_{1P} + k_{2P} x_9} T_2^0 - d_{T_2} x_6, \\
f_7(x) = \lambda_{C_1} x_5 - k_{C_1N_1} x_7 x_1 - d_{C_1} x_7, \\
f_8(x) = \lambda_{C_2} x_6 - k_{C_2N_2} x_8 x_2 - d_{C_2} x_8, \\
f_9(x) = \lambda_{C_4M_1} \frac{1}{k_{C_4} + x_{10}} x_3 - d_{C_3} x_9, \\
f_{10}(x) = \lambda_{C_4} x_4 - d_{C_4} x_{10},
\end{cases}$$

and observe that F satisfies the quasi-positivity property, that is, for all indices $i \in \{1, ..., 10\}$

we have

$$\forall (x_j)_{j\neq i} \in (\mathbf{R}^+)^9,\ f_i(x_1,...,x_{i-1},0,x_{i+1},...,x_{10}) \geq 0.$$

Thus, from Proposition 2.1 in Haraux [63], we conclude that the solution remains non-negative because of this property.

The solution is bounded because from the fourteenth equation of system (2.1)-(2.10), we can conclude that under the assumption that $M_2(0) > 0$ and if C_4 is large enough then $\frac{dC_4}{dt} < 0$ and, therefore, $C_4(t)$ remains bounded. By reapplying the same argument, we subsequently conclude the same result for the rest of the variables of the system. Since the solutions of system (2.1)-(2.10) are bounded, they are defined for all $t > 0$. □

2.2. Reduced inflammation model

In order to study pattern formation in the model of inflammation, we will formally reduce system (2.1)-(2.10) to a system of two equations. This reduction is based on the approximations of detailed equilibrium for some variables (fast and slow variables) and on the assumption that some constants are small ($k_{C_1N_1}, k_{C_2N_2}$) and the corresponding terms can be neglected (k_{2P}). The effect of C_1 and C_2 cytokines in the differentiation of monocytes to macrophages are neglected. In fact, the differentiation of monocytes into macrophages is described as a slow and progressive event [64]. The development of inflammation directly influence the differentiation of T-cells [65] leading to a rapid increase in their concentrations, hence we neglect the saturation in the influx of T-helper cells. The simplified model provides a starting point for further investigations of the complete model without these assumptions.

Equating zero the right-hand side of equation (2.3), we get

$$M_1 = \frac{\lambda_{C_1N_1}}{d_{M_1}} \frac{C_1N_1}{k_{C_1} + C_1 + k_4C_4}\,. \tag{2.11}$$

Similar, from equation (2.4),

$$M_2 = \frac{\lambda_{C_2N_2}}{d_{M_2}} \frac{C_2N_2}{k_{N_2} + C_2}\,. \tag{2.12}$$

From equations (2.7), (2.8) for $k_{C_1N_1} = k_{C_2N_2} = 0$,

$$C_1 = \frac{\lambda_{C_1}}{d_{C_1}}\, T_1\,, \quad C_2 = \frac{\lambda_{C_1}}{d_{C_1}}\, T_2\,. \tag{2.13}$$

Next, approximating P by C_3, we get from equations (2.5) and (2.6) for $k_{2P} = 0$:

$$T_1 = \frac{\lambda_{PT_1}T_1^0}{k_{1P}d_{T_1}}\, C_3\,, \quad T_2 = \frac{\lambda_{PT_2}T_2^0}{k_{1P}d_{T_2}}\, C_3\,. \tag{2.14}$$

As before, we find from equations (2.1), (2.2):

$$N_1 = \frac{\lambda_{PN_1}N_1^0}{k_{1P}d_{N_1}}\, C_3\,, \quad N_2 = \frac{\lambda_{PN_2}N_2^0}{k_{1P}d_{N_2}}\, C_3\,. \tag{2.15}$$

Finally, substituting all these relations in equations (2.9), (2.10) we get:

$$\frac{dC_3}{dt} = \frac{a_1 C_3^2}{1 + a_2 C_3 + a_3 C_4} - \sigma_1 C_3, \tag{2.16}$$

$$\frac{dC_4}{dt} = \frac{b_1 C_3^2}{1 + b_2 C_3} - \sigma_2 C_4, \tag{2.17}$$

where parameters a_i, b_i, σ_i can be expressed through the original parameters. This model will be analyzed in the next section.

3. Pattern formation

3.1. Analysis of non-spatially-distributed system

Denoting for convenience $A = C_3$, $B = C_4$, we obtain the non-spatially-distributed system, considered in this section:

$$\begin{cases} \dfrac{dA}{dt} = \dfrac{a_1 A^2}{1 + a_2 A + a_3 B} - \sigma_1 A, \\ \\ \dfrac{dB}{dt} = \dfrac{b_1 A^2}{1 + b_2 A} - \sigma_2 B, \end{cases} \tag{3.1}$$

all the parameters of which are positive. The nullclines of the system (3.1) are

$$A = 0\,, \quad B = \frac{1}{a_3}\left(\left(\frac{a_1}{\sigma_1} - a_2\right)A - 1\right), \qquad B = \frac{b_1 A^2}{\sigma_2(1 + b_2 A)}. \tag{3.2}$$

The first nullcline, referred to as A-nullcline, is a pair of lines, intersecting at $(0, -1/a_3)$. The second nullcline, B-nullcline, is a hyperbola with the asymptotes $A = -1/b_2$, always situated in the left half-plane, and $B = (b_1/b_2\sigma_2)A - b_1/b_2^2\sigma_2$, always has a positive slope and intersects the ordinate axis in the lower half-plane. B-nullcline goes through the point $(0,0)$, touching the abscissa axis at it, and it has a positive second derivative equal to $2b_1/\sigma_2$.

The system (3.1) has a stationary state $(0,0)$ for all values of parameters. As Figure 2 illustrates, depending on the values of parameters, the system can have one or two stationary states in the first quadrant, where the solutions have physical meaning. Note that the phase vectors are not defined at the lines $A = -1/b_2$ and $B = -(1 + a_2 A)/a_3$ where one of the denominators of system (3.1) vanish, but they do not belong to the first quadrant.

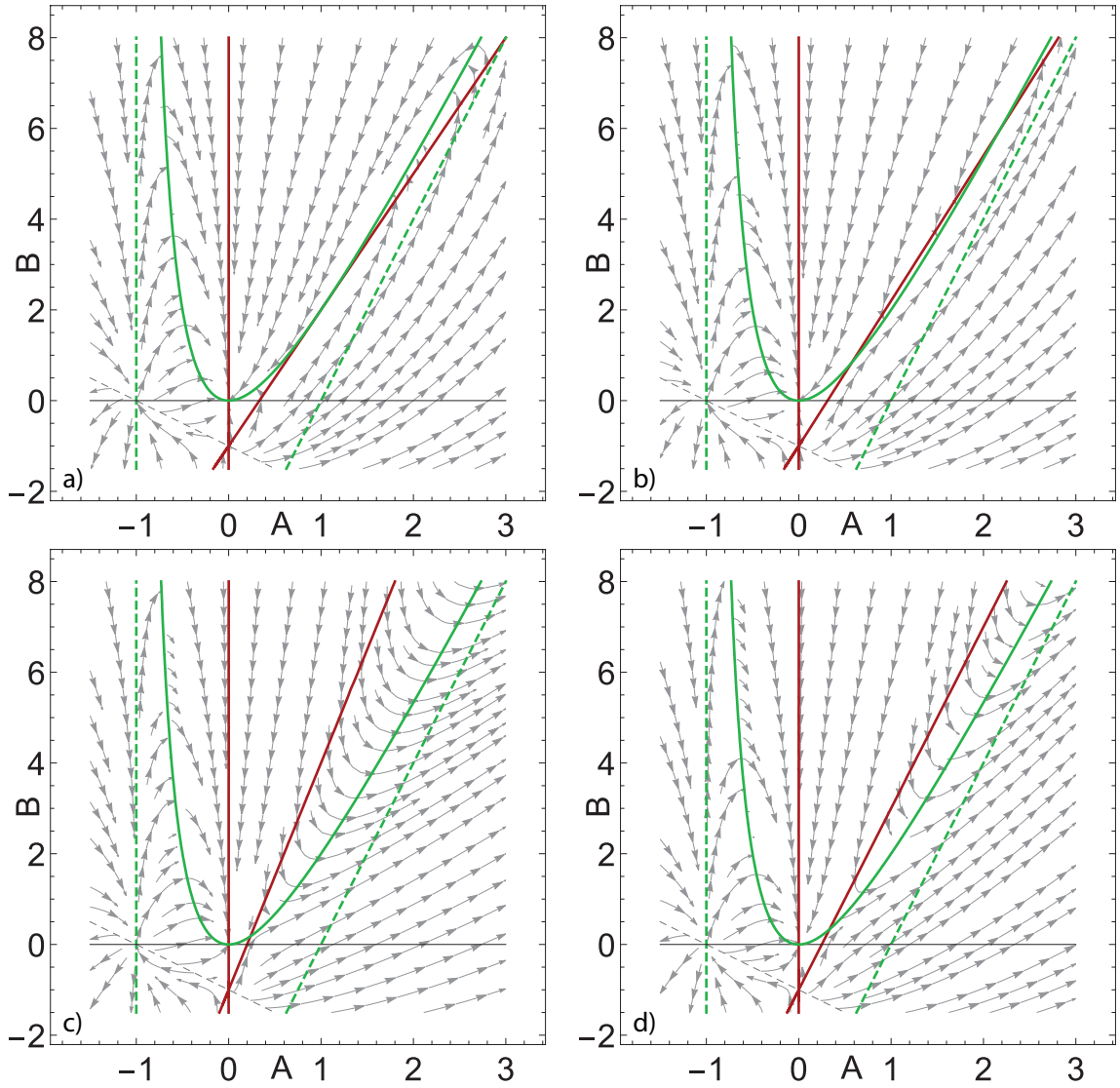

Figure 2. Phase portraits of the system (3.1) under the values of parameters $a_2 = a_3 = b_2 = \sigma_1 = \sigma_2 = 1$, $b_1 = 4$ and a_1, equal to a) 4, b) 4.2, c) 6, d) 5. Red lines are A-nullclines, green solid lines are B-nullclines, green dashed lines are its asymtpotes. Gray solid lines are abscissa axes, gray dashed lines along with the vertical asymptotes are the sets, where the phase vectors are not defined.

In order to identify the parameter region, where the system has one or two stationary states in the first quadrant, it is useful first of all to retrieve the conditions, under which the nullclines touch each other in the first quadrant. They can be obtained by consideration of the following system, which respresent the conditions, that the nullclines have the same first derivative at their common point:

$$\begin{cases} \dfrac{1}{a_3}\left(\left(\dfrac{a_1}{\sigma_1} - a_2\right)A - 1\right) = \dfrac{b_1 A^2}{\sigma_2(1+b_2A)}, \\ \dfrac{1}{a_3}\left(\dfrac{a_1}{\sigma_1} - a_2\right) = \dfrac{b_1 A(2+b_2A)}{\sigma_2(1+b_2A)^2}. \end{cases}$$

Its straightforward transformation gives the following conditions for the touching of the

nullclines in the first quadrant (see example in Figure 2a):

$$\begin{cases} \dfrac{a_1}{\sigma_1} > a_2 + b_2, \\ \dfrac{a_1}{\sigma_1} = 2\sqrt{\dfrac{a_3 b_1}{\sigma_2}} + a_2 - b_2. \end{cases} \tag{3.3}$$

From the geometrical reasoning it is clear that there are two stationary states in the first quadrant if the slope of the second line of A-nullcline is greater than the slope in the case of touching the B-nullcline, but not greater than the slope of its asymptote (see Figure 2b):

$$\begin{cases} \dfrac{a_1}{\sigma_1} > a_2 + b_2, \\ \dfrac{a_3 b_1}{b_2 \sigma_2} + a_2 > \dfrac{a_1}{\sigma_1} > 2\sqrt{\dfrac{a_3 b_1}{\sigma_2}} + a_2 - b_2. \end{cases} \tag{3.4}$$

The case of one stationary state in the first quadrant, apart from the case of touching of nullclines, described by Equation (3.3), is realised in the situation, when the slope of the second line of A-nullcline is greater than the slope of the asymptote of the B-nullcline (see Figure 2c):

$$\frac{a_1}{\sigma_1} > \frac{a_3 b_1}{b_2 \sigma_2} + a_2, \tag{3.5}$$

or in a borderline situation, when their slopes are equal, but the second line of A-nullcline lies higher than the asymptote of the B-nullcline (see Figure 2d):

$$\begin{cases} \dfrac{a_1}{\sigma_1} = \dfrac{a_3 b_1}{b_2 \sigma_2} + a_2, \\ \\ \dfrac{a_3 b_1}{b_2^2 \sigma_2} > 1. \end{cases} \tag{3.6}$$

Stability of the stationary state $(0,0)$ can be studied using the Jacobian matrix at the stationary state $(0,0)$:

$$\begin{pmatrix} -\sigma_1 & 0 \\ 0 & -\sigma_2 \end{pmatrix}, \tag{3.7}$$

which indicates that this point is always a stable node. According to the second Poincaré Index Theorem [66], the neighbouring simple stationary state along the B-nullcline can be only a saddle. Therefore, in the cases of one stationary state in the first quadrant, described by Equation (3.5) and (3.6), this state in always unstable. In the case of two stationary states in the first quadrant, described by Equation (3.4), the state with smaller coordinates is also unstable. The stability of the stationary state with greater coordinate is a less trivial question, and it seems to be dependent on the specific values of parameters. Further we will consider the case, corresponding to Figure 2, fixing the values $a_2 = a_3 = b_2 = \sigma_1 = \sigma_2 = 1$, $b_1 = 4$, and varying the value of a_1. In this case, there exist a stable stationary state in the region $4 < a_1 < 5$:

$$\begin{aligned} A_S(a_1) &= \frac{a_1 - 2 + \sqrt{a_1^2 - 16}}{2(5 - a_1)}, \\ B_S(a_1) &= \frac{a_1^2 - a_1 - 8 + [a_1 - 1]\sqrt{a_1^2 - 16}}{2(5 - a_1)}, \end{aligned} \tag{3.8}$$

that can be checked by straightforward calculations. This state corresponds to persistent inflammation under strong enough activation of corresponding cytokines.

3.2. Turing structures in a spatially-distributed system

In this section, we consider a spatially-distributed system

$$\begin{cases} \dfrac{\partial A}{\partial t} = \dfrac{a_1 A^2}{1 + A + B} - A + \Delta A, \\ \dfrac{\partial B}{\partial t} = \dfrac{4A^2}{1 + A} - B + D_B \Delta B, \end{cases} \tag{3.9}$$

focusing on the formation of stationary non-uniform structures in it, i.e., the Turing patterns. Their emergence is determined by the system linearized at a corresponding stationary state [37]. For simplicity of calculations, we set here $a_2 = a_3 = 1, b_1 = 4, b_2 = 1, \sigma_1 = \sigma_2 = 1$, and consider a_1 as a parameter of the problem. In general case of a system

$$\begin{cases} \dfrac{\partial \widetilde{A}}{\partial t} = a_{11}\widetilde{A} + a_{12}\widetilde{B} + D_1 \Delta \widetilde{A}, \\ \dfrac{\partial \widetilde{B}}{\partial t} = a_{21}\widetilde{A} + a_{22}\widetilde{B} + D_2 \Delta \widetilde{B}, \end{cases} \tag{3.10}$$

where $\widetilde{A}$ and $\widetilde{B}$ denote the perturbations of the stationary state, the conditions for Turing instability can be formulated in the following way:

$$\begin{cases} a_{11}a_{22} - a_{12}a_{21} > 0, \\ a_{11} + a_{22} < 0, \\ D_2 a_{11} + D_1 a_{22} - 2\sqrt{D_1 D_2 (a_{11}a_{22} - a_{12}a_{21})} > 0. \end{cases} \tag{3.11}$$

The first two inequalities ensure stability of a corresponding stationary state in the absence of diffusion, while the third condition indicates that in its presence the modes with some wavelengths become unstable, eventually producing a non-uniform stationary pattern. Of note, the formation of Turing structures in the considered system (3.9) is impossible around the uniform stationary state $(0,0)$ due to the fact, that both variables there act as self-inhibitors, down-regulating their own production at the uniform stationary state, which follows from Eq. (3.7).

As it was mentioned in Section 3.1, in the region $4 < a_1 < 5$ there exists a stationary state with coordinates $A_S > 0$, $B_S > 0$, which is stable in the absence of diffusion implying

the fulfillment of the first two conditions for Turing instability around this state. The third condition, applied to the system (3.9), turns into the inequality

$$\frac{a_1-1}{a_1}D_B - 2\sqrt{\frac{-a_1^2+16+[8-a_1]\sqrt{a_1^2-16}}{8a_1}D_B - 1} > 0.$$

Figure 3 depicts the part of the region in the parametric space where this condition is also fulfilled, and the formation of the Turing patterns can take place. Note that the diffusion coefficients should not differ very much, i.e., the value of $D_B = 2.64$ already results in the Turing instability for every considered value of a_1. This is crucial from the biological point of view, since diffusivities of different cytokines can hardly differ an order of magnitude or more under identical conditions.

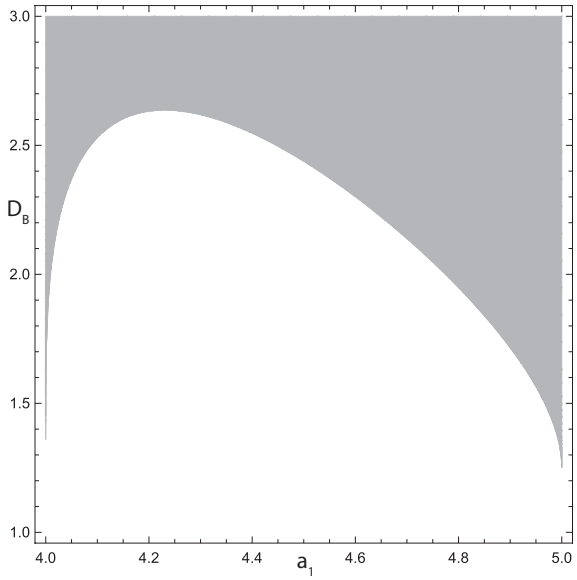

Figure 3. Gray area denotes the region of Turing instability of the system (3.9) which continues with increase in D_B.

3.3. Numerical simulations and results

Turing patterns formation for the considered system was studied numerically in the two-dimensional square domain. The size of the domain $L = 200$ was chosen to be sufficiently large in order for several of the unstable wavelengths to fit it under any of the used parameter sets. As initial conditions we consider a sufficiently strong local perturbation of the form

$$A(x,y) = B(x,y) = 10\left(1+10((x-L/2)^2+(y-L/2)^2)\right)^{-1}$$

which corresponds to the local initiation of the plaque formation process. The simulations were performed with the C++ implemented code. Zero flux conditions were considered at the boundaries. The equations were solved using the method of splitting into physical processes, i.e., at each time step, the reaction and diffusion terms were calculated sequentially. The space step was chosen to be sufficiently small to correctly reproduce the emerging structures; the time step was chosen in order to minimize the computation time while maintaining the

functionality of the implicit Crank-Nicholson method, used to solve the diffusion equations, and the fourth order Runge-Kutta method, used to solve the reaction equations. It was verified that the refinement of discretization does not qualitatively affect the result.

Table 1. Values of parameters used in numerical simulations for the considered system (3.9). The values of D_B and a_1 are varying and denoted under each numerical figure.

Parameter	Value	Biological description
a_2	1	Saturation in the production of A
a_3	1	Inhibition rate in the production of A due to B
b_1	4	Production of cytokines B due to the presence of cytokines A
b_2	1	Inhibition rate in the production of B due to A
σ_1	1	Death rates of cytokines A
σ_2	1	Death rates of cytokines B

An important moment is that numerical simulations of the considered system (3.9) demonstrated unrestrained growth of solutions under sufficiently high values of D_B and a_1. This is related to the fact that the model describes only the initial stage of inflammation progression. There are various other anti-inflammatory mechanisms initiated at more advanced stages of inflammation [67, 68]. Moreover, there are some simplifying assumptions in the model, such as cell influx is not limited and cytokines production is a linear function of cell concentration without limitation mechanisms. In order to implicitly account for the fact of restrained inflammation growth, the following restrictions were introduced and implemented within the program code:

$$\begin{aligned}
\frac{\partial A}{\partial t} &= \begin{cases} \dfrac{a_1 A^2}{1+A+B} - A + \Delta A \;\; if \;\; A < k_{lim} A_S(a_1), \\ 0 \;\; if \;\; A \geq k_{lim} A_S(a_1); \end{cases} \\
\frac{\partial B}{\partial t} &= \begin{cases} \dfrac{4A^2}{1+A} - B + D_B \Delta B \;\; if \;\; B < k_{lim} B_S(a_1), \\ 0 \;\; if \;\; B \geq k_{lim} B_S(a_1); \end{cases}
\end{aligned} \tag{3.12}$$

the functions of $A_S(a_1)$ and $B_S(a_1)$ being defined in Equation (3.8). The value of the constant k_{lim} is considered as a parameter.

Figure 4 shows the dynamics of Turing patterns formation under $k_{lim} = 2$ for different values of parameters D_B and a_1, the most right snapshots displaying visually stabilized patterns. Depending on the parameter values, the considered system can exhibit several qualitatively different ways of self-completion of initial local excitation into Turing patterns. Some aspects of the shown dynamics correspond to the ones, previously reported for other classical nonlinear systems [69–71].

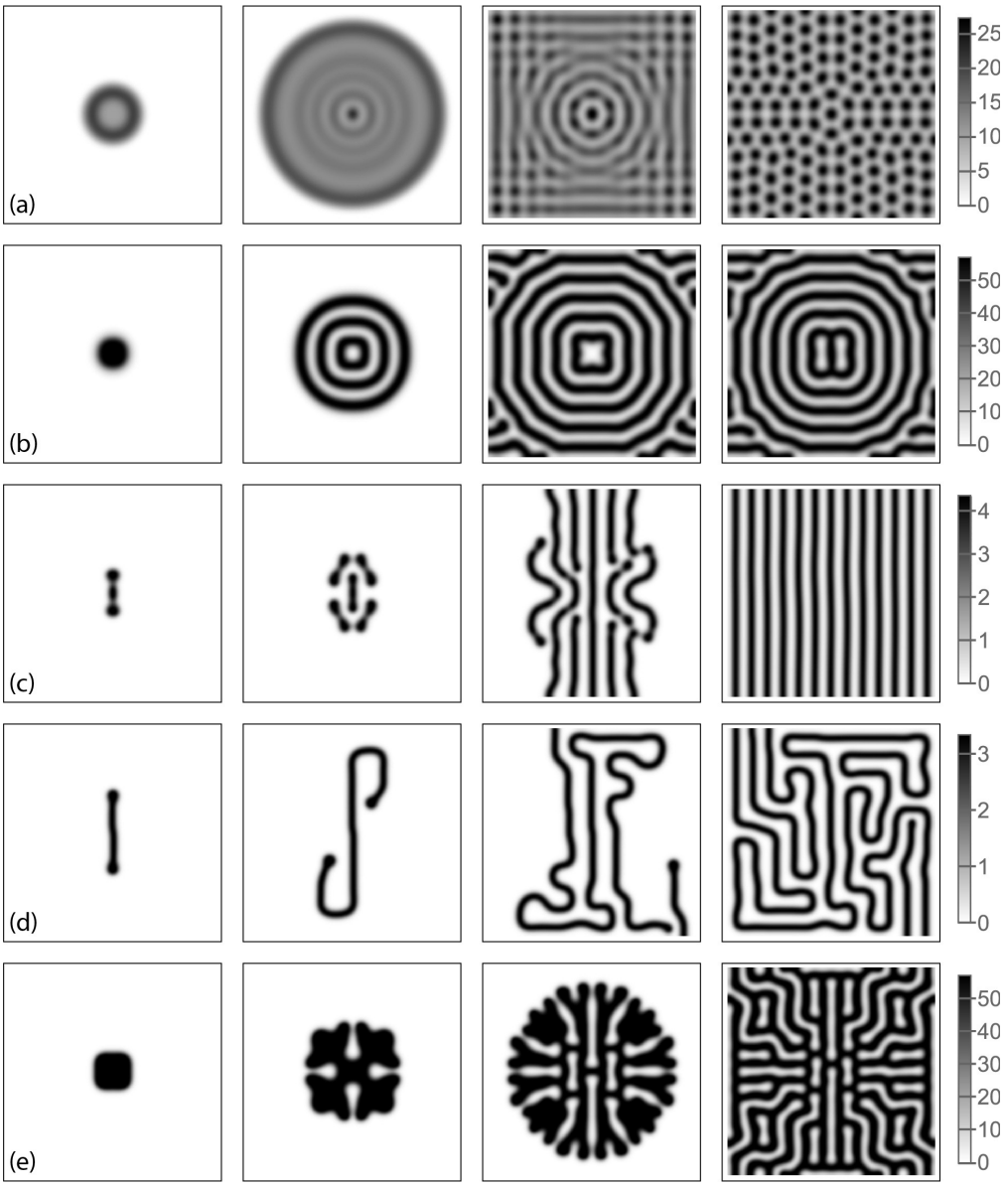

Figure 4. Dynamics of Turing patterns formation in the system (3.12), $k_{lim} = 2$. Variable A is shown. Parameters and time values (from left to right) are: (a) $D_B = 2$, $a_1 = 4.8$; t=200, 400, 800, 3500; (b) $D_B = 2$, $a_1 = 4.9$; t=200, 400, 1200, 3500; (c) $D_B = 3$, $a_1 = 4.2$; t=500, 900, 4700, 16000; (d) $D_B = 3.5$, $a_1 = 4.1$; t=100, 300, 7500, 35000; (e) $D_B = 3$, $a_1 = 4.9$; t=200, 400, 600, 6500.

Close to the boundary of the Turing instability region under low values of D_B, the spot-like structures eventually appear. In this case, as shown in Figure 4a, initial excitation results in the propagation of a circular wave, and the values of model variables in its interior region oscillate around the stationary state A_S, B_S. The spots close to the initial excitation arise in result of the rotational symmetry breaking of these oscillatory tails. The positions of the spots, situated further from the initial excitation, are strongly affected by their proximity to the boundaries of the computational domain. Under higher values of a_1, as Figure 4b demonstrates, the rotational symmetry breaking does not happen and the resulting patterns represent concentric circles, deformed due to the boundary effects.

Deeper in the Turing instability region, the nature of the patterns changes drastically. Under higher values of D_B and sufficiently low values of a_1, this process begins with the elongating

of the initial spot in one direction, along which it has a slightly increased ratio of activator to inhibitor. The evolution of the developed snakelike structures, that can tear, corrugate and fuse together, may result in stripes, aligned in one direction, as illustrated by Figure 4c, or in labyrinth patterns, as exemplified by Figure 4d, as well as in various transient patterns. Under sufficiently high values of a_1 the initial excitation transforms into thick spot, which develops into Turing pattern via consecutive symmetry breaking, as Figure 4e shows.

Interestingly, the choice of the value of k_{lim} by itself affects the form of the emerging patterns. For example, Figure 5a shows the evolution of the considered system under the values of model parameters, corresponding to Figure 4c, but under greater value of $k_{lim} = 3$. In this case, the spot-like structures begin to break apart after the initial elongation, eventually resulting in a domain covered in spots, rather than parallel stripes. Under further increase of k_{lim} for the same values of D_B and a_1, the initially formed spot-like structure becomes much more stable and retains its shape during the numerical simulation (at least until $t = 35000$). However, such localized structure can be perturbed by external noise. Sufficiently strong noise can result in displacement of the structure, and even stronger noise can lead also to its self-completion. Figure 5b illustrates the corresponding numerical simulation, where the random number in the range $[-0.5; 0.5]$ is added to the values of both variables at every grid point at every time step. Note that during the simulation these perturbations once add up to disturbance sufficiently strong to initiate a new localized structure near the left boundary.

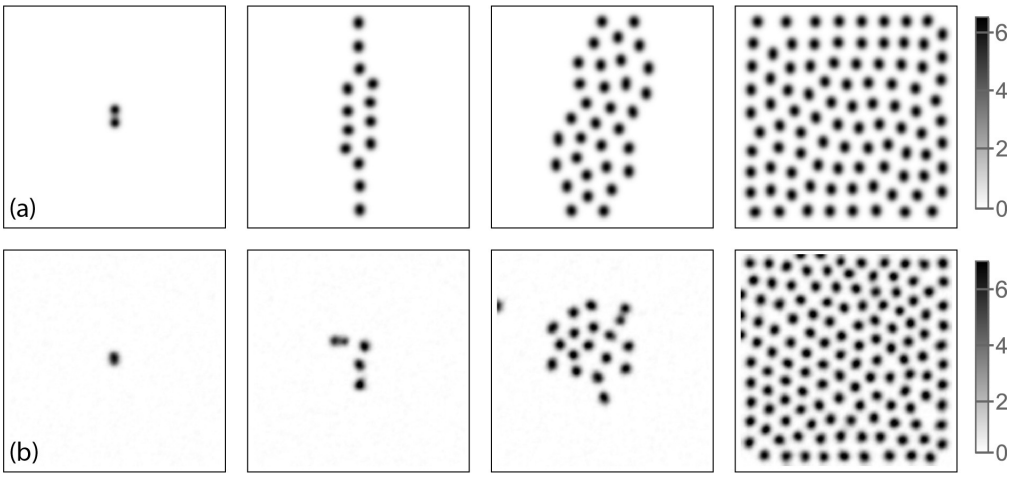

Figure 5. Dynamics of Turing patterns formation in the system (3.9) under $D_B = 3$, $a_1 = 4.2$. Variable A is shown. Restriction parameter and time values (from left to right) are: (a) $k_{lim} = 3$; t=60, 1500, 3000, 8000; (b) $k_{lim} \to \infty$; t=60, 200, 400, 1300; the system evolves under additional noise (see text).

4. Discussion and Conclusion

We suggest in this work a generic model of inflammation, which includes the main cell types involved in this process, and pro- and anti-inflammatory cytokines. After some simplifications, we reduce this model to a two-equation model since the analysis of the complete model would be excessively difficult, and it would not give an analytical result.

Inflammatory diseases. Inflammation is a complex physiological process including many cell types, cytokines and chemokines with multiple interactions between them and various

positive and negative feedbacks. We can represent these multiple factors as two big groups, pro-inflammatory and anti-inflammatory factors. Pro-inflammatory factors stimulate their own production and the production of anti-inflammatory factors, while the latter downregulate the production of both of them. This kind of interaction together with diffusion (or random motion for cells) can result in a non-homogeneous spatial distribution of these factors leading to the formation of lesions (or plaques). Inflammatory skin diseases manifest spectacular examples of different plaques. Among them, linear, target, multiform and serpiginous plaques, which are also observed in modelling results (Figures 6, 8).

We hypothesize that the interaction of pro- and anti-inflammatory factors determine the lesion shape, size, and growth rate. Mathematical modelling shows that in the presence of only pro-inflammatory factors, the lesion grows as a single circular plaque, which is not the case for the majority of patients. The presence of different plaque forms (Figures 6–8) confirms the hypothesis about the role of anti-inflammatory factors in their formation.

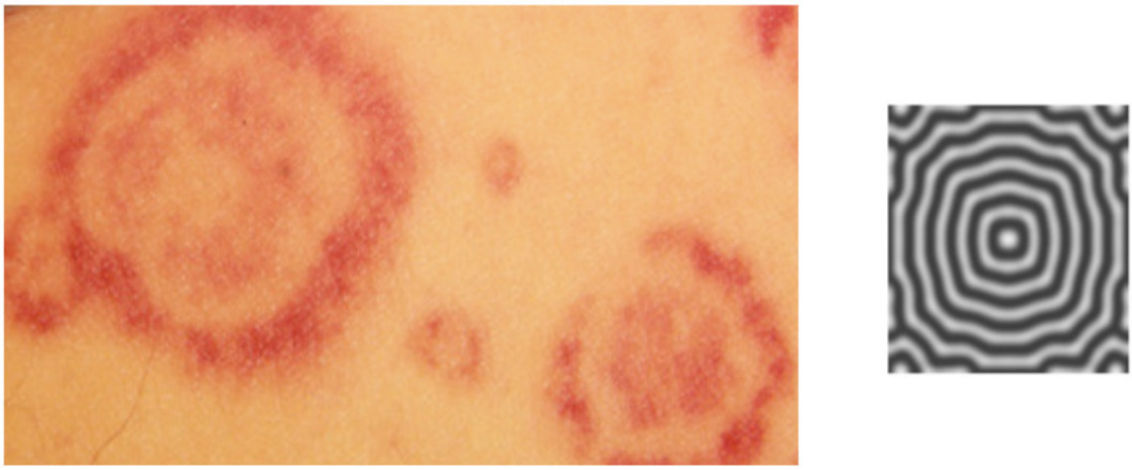

Figure 6. Target (middle) and numerical simulations. Left figure is taken from: https://www.dermnetnz.org/topics/terminology. Let us also indicate serpiginous plaques in Figure 4 (d).

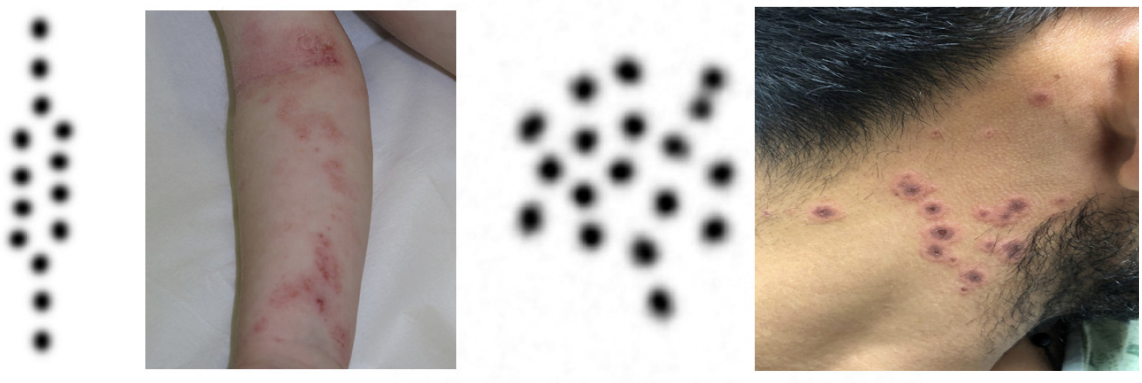

Figure 7. Linear (left), and multiform (right) skin lesions and numerical simulations. Source for the left figure: A linear lesion in a child with atopic dermatitis: Not a coincidence, 2019 [72]. Source for the right figure: Variants of Erythema Multiforme: A Case Report and Literature Review, 2018 [73].

We provide a qualitative comparison between the numerical results obtained in Figures 5

and 4 and skin lesions observed in eczema as a specific disease case. Figure 6 shows target lesions and the corresponding patterns obtained in numerical simulations. Figure 7 shows linear and multiform lesions and the corresponding patterns obtained in numerical simulations. We note that the figures are taken from case reports of skin diseases [72, 73]. Figure 8 presents drawings of some other lesions with different structures. Most of them have some similarities with the simulated structures. Cases 1 and 7 correspond to stripe patterns c, case 3 to single dot and case 5 to multiple dot patterns a and b. Case 6 resembles the transient cross pattern e (right), and case 8 the labyrinth pattern d.

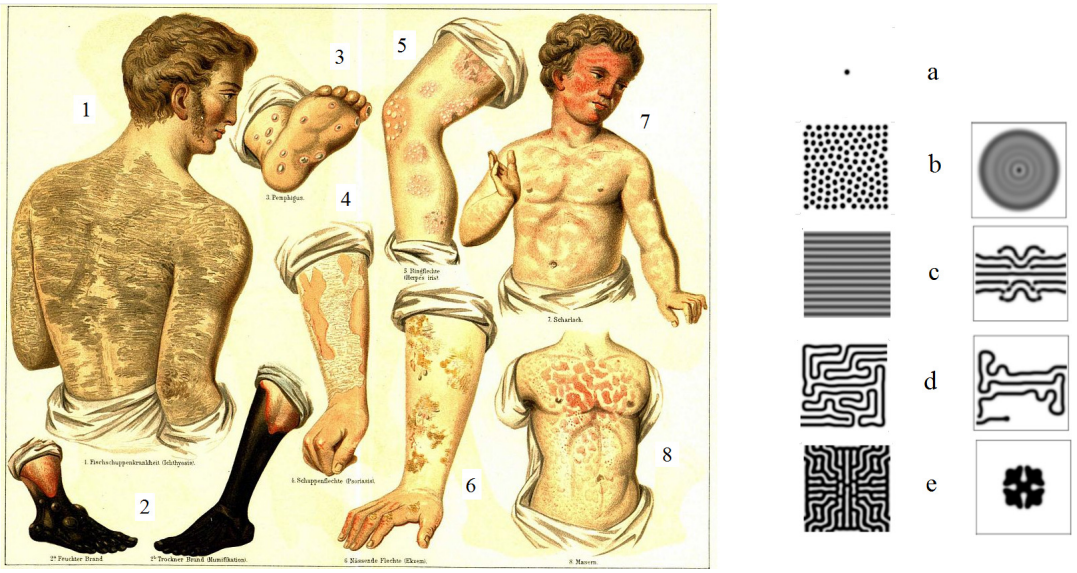

Figure 8. Left: different forms of skin lesions. Source: "Maladies de la peau", vol. 8 of the 4th edition of Meyers Konversations-Lexikon, (1885–90) ,https://fr.wikipedia.org/wiki/Eczema. Right: different patterns in numerical simulations (the values of parameters are given in the appendix). Final patterns are shown in the left column and the corresponding transient patterns in the right column. Skin lesions shown at the left correspond to some of the numerical patterns: 1 - c (left), 3 - a, 5 - b (left), 6 - e (right), 7 - c (right), 8 - d (left).

Short range activation - long range inhibition. Conditions of the emergence of dissipative structures imply that the diffusion coefficient of inhibitor is greater than the diffusion coefficient of activator. Activating and inhibiting pathways include cells (monocytes, macrophages, foam cells, smooth muscle cells, T-helper cells) and cytokines. Molecular weights of pro-inflammatory cytokines (IL-6 - 26 kDa, IL-12 - 70 kDa, TNF-α - 17.3 kDa) is an average greater that of anti-inflammatory cytokines (IL-10 - 18 kDa, TGF-β (active form) - 12 kDa). Since the diffusion coefficient is in inverse proportion to the power $1/3$ of molecular weight, then anti-inflammatory cytokines diffuse faster. We can highlight that the motion of pro-inflammatory and anti-inflammatory macrophages can be tackled in future works.

Wave propagation. Reduced inflammatory model developed in this work has from one to three non-negative stationary points. Their number and stability depend on the parameters of the model. Besides stable zero stationary point, the model can have one more stable and unstable points. Therefore, it is a bistable case, and the transition from the disease-free stationary point to a disease stationary point occurs if the initial perturbation is sufficiently large.

If we consider a spatially distributed system with a localized in space initial perturbation

of the disease-free equilibrium, then transition to the disease equilibrium occurs in the form of travelling waves. Existence and stability of such waves in the two-equation pro-inflammatory system was studied in [27]. Transition waves for more complete pro- and anti-inflammatory systems will be studied in the subsequent works. Let us only mention here that in the pro-inflammatory model the disease equilibrium is stable. Wave propagation describes growth of a single circular plaque. In the case of pro- and anti-inflammatory model, the disease equilibrium can become unstable. In this case, the solution behind the wave is non-homogeneous in space, and we obtain multiple plaques with different shapes.

Random perturbations of cell and cytokines concentrations specific for physiological systems can be essential at the initial stage of the set-up of inflammation. After the initiations, small randomly located lesions can merge and form a single lesions, as it is the case of the process is dominated by pro-inflammatory factors, or they can evolve to multiple lesions with complex structures under the influence of anti-inflammatory factors.

Limitations and perspectives. Studying inflammatory diseases, we encounter the usual difficulties of the biomedical modelling: physiological processes are too complex, they contain many unknown or partially known factors, the values of kinetic parameters are basically unknown. In this case, we have to rely on qualitative models which are in agreement with established physiological data. We have to simplify the model grouping them into two classes, pro- and anti-inflammatory. This work can be considered as an initial qualitative model to describe pattern formation in skin diseases. Further works can be implemented to compare those results to experimental data and to provide quantitative interpretation of the results.

Some of the kinetic constants are estimated in the literature, some other are considered as free parameters and varied in numerical simulations. Generic inflammatory model, obtained by a formal reduction from a more complete model, contains a relatively small number of parameters. Their values are chosen from the conditions of the emergence of spatial structures. The application of these qualitative ideas and results to specific inflammatory diseases will require further investigations.

Acknowledgments

The last author has been supported by the RUDN University Strategic Academic Leadership Program.

Conflicts of Interests

The authors declare no conflict of interest.

Authors contribution

Conceptualization, Wissam El Hajj, Maxim Kuznetsov and Vitaly Volpert; Formal analysis, Wissam El Hajj; Methodology, Maxim Kuznetsov and Vitaly Volpert; Software, Maxim Kuznetsov; Validation, Vitaly Volpert; Writing – original draft, Wissam El Hajj, Maxim Kuznetsov and Vitaly Volpert; Writing – review & editing, Wissam El Hajj and Vitaly Volpert; Visualization, Maxim Kuznetsov; Supervision, Vitaly Volpert; Project administration, Vitaly

Volpert. All authors have read and agreed to the published version of the manuscript.

References

[1] Chovatiya R, Medzhitov R. Stress, inflammation, and defense of homeostasis. *Mol. Cell* 2014, 54(2):281–288.

[2] Chen L, Deng H, Cui H, Fang J, Zuo Z, *et al.* Inflammatory responses and inflammation-associated diseases in organs. *Oncotarget* 2018, 9(6):7204–7218.

[3] Marchi S, Guilbaud E, Tait SWG, Yamazaki T, Galluzzi L. Mitochondrial control of inflammation. *Nat. Rev. Immunol.* 2023, 23(3):159–173.

[4] Shi C, Pamer EG. Monocyte recruitment during infection and inflammation. *Nat. Rev. Immunol.* 2011, 11(11):762–774.

[5] Ma Z, Du B, Li J, Yang Y, Zhu F. An insight into anti-inflammatory activities and inflammation related diseases of anthocyanins: A review of both in vivo and in vitro investigations. *Int. J. Mol. Sci.* 2021, 22(20):11076.

[6] Singh N, Baby D, Rajguru J, Patil P, Thakkannavar S, *et al.* Inflammation and cancer. *Ann. Afr. Med.* 2019, 18(3):121–126.

[7] Henein MY, Vancheri S, Longo G, Vancheri F. The role of inflammation in cardiovascular disease. *Int. J. Mol. Sci.* 2022, 23(21):12906.

[8] Tampa M, Neagu M, Caruntu C, Constantin C, Georgescu SR. Skin inflammation—A cornerstone in dermatological conditions. *J. Pers. Med.* 2022, 12(9):1370.

[9] Bayik D, Tross D, Haile LA, Verthelyi D, Klinman DM. Regulation of the maturation of human monocytes into immunosuppressive macrophages. *Blood Adv.* 2017, 1(26):2510–2519.

[10] Bartlett B, Ludewick HP, Misra A, Lee S, Dwivedi G. Macrophages and T cells in atherosclerosis: a translational perspective. *Am. J. Physiol. Heart Circ. Physiol.* 2019, 317(2):H375–H386.

[11] Tabas I, Lichtman AH. Monocyte-macrophages and T cells in atherosclerosis. *Immunity* 2017, 47(4):621–634.

[12] Mills CD. M1 and M2 macrophages: Oracles of health and disease. *Crit. Rev. Immunol.* 2012, 32(6):463–488.

[13] Arango Duque G, Descoteaux A. Macrophage cytokines: involvement in immunity and infectious diseases. *Front. Immunol.* 2014, 5:491.

[14] Wojdasiewicz P, Poniatowski LA, Szukiewicz D. The role of inflammatory and anti-inflammatory cytokines in the pathogenesis of osteoarthritis. *Mediators Inflamm.* 2014, 2014:1–19.

[15] Schuerwegh AJ, Dombrecht EJ, Stevens WJ, Van Offel JF, Bridts CH, *et al.* Influence of

pro-inflammatory (IL-1α, IL-6, TNF-α, IFN-γ) and anti-inflammatory (IL-4) cytokines on chondrocyte function. *Osteoarthr. Cartilage* 2003, 11(9):681–687.

[16] Tanghetti EA. The role of inflammation in the pathology of acne. *J. Clin. Aesthet. Dermatol.* 2013, 6(9):27–35.

[17] Brown SJ. Atopic eczema. *Clin. Med.* 2016, 16(1):66–69.

[18] Diotallevi F, Offidani A. Skin, autoimmunity and inflammation: A comprehensive exploration through scientific research. *Int. J. Mol. Sci.* 2023, 24(21):15857.

[19] Sroka-Tomaszewska J, Trzeciak M. Molecular mechanisms of atopic dermatitis pathogenesis. *Int. J. Mol. Sci.* 2021, 22(8):4130.

[20] Sawada Y, Saito-Sasaki N, Mashima E, Nakamura M. Daily lifestyle and inflammatory skin diseases. *Int. J. Mol. Sci.* 2021, 22(10):5204.

[21] Dainichi T, Hanakawa S, Kabashima K. Classification of inflammatory skin diseases: A proposal based on the disorders of the three-layered defense systems, barrier, innate immunity and acquired immunity. *J. Dermatol. Sci.* 2014, 76(2):81–89.

[22] Yoshimura A, Aki D, Ito M. SOCS, SPRED, and NR4a: Negative regulators of cytokine signaling and transcription in immune tolerance. *Proc. Jpn. Acad. Ser. B Phys. Biol. Sci.* 2021, 97(6):277–291.

[23] Cianciulli A, Calvello R, Porro C, Lofrumento DD, Panaro MA. Inflammatory skin diseases: Focus on the role of suppressors of cytokine signaling (SOCS) proteins. *Cells* 2024, 13(6):505.

[24] Beck LA, Cork MJ, Amagai M, De Benedetto A, Kabashima K, *et al.* Type 2 inflammation contributes to skin barrier dysfunction in atopic dermatitis. *JID Innov.* 2022, 2(5):100131.

[25] Herald MC. General model of inflammation. *Bull. Math. Biol.* 2010, 72(4):765–779.

[26] Nikaein N, Tuerxun K, Cedersund G, Eklund D, Kruse R, *et al.* Mathematical models disentangle the role of IL-10 feedbacks in human monocytes upon proinflammatory activation. *J. Biol. Chem.* 2023, 299(10):105205.

[27] El Khatib N, Genieys S, Volpert V. Atherosclerosis initiation modeled as an inflammatory process. *Math. Modell. Nat. Phenom.* 2007, 2(2):126–141.

[28] El Hajj W, El Khatib N, Volpert V. Inflammation propagation modeled as a reaction-diffusion wave. *Math. Biosci.* 2023, 365:109074.

[29] Abi Younes G, El Khatib N. Mathematical modeling of inflammatory processes of atherosclerosis. *Math. Model. Nat. Phenom.* 2022, 17:5.

[30] El Hajj W, El Khatib N. Effect of permeability on the initiation of Atherosclerosis modeled as an inflammatory process. *J. Theor. Biol.* 2023, 564:111461.

[31] Bozkurt F, Yousef A, Bilgil H, Baleanu D. A mathematical model with piecewise constant

arguments of colorectal cancer with chemo-immunotherapy. *Chaos Soliton. Fract.* 2023, 168:113207.

[32] Tanaka RJ, Ono M. Skin Disease Modeling from a Mathematical Perspective. *J. Invest. Dermatol.* 2013, 133(6):1472–1478.

[33] Nakaoka S, Kuwahara S, Lee C, Jeon H, Lee J, *et al.* Chronic inflammation in the epidermis: A mathematical model. *Appl. Sci. (Basel)* 2016, 6(9):252.

[34] Valeyev NV, Hundhausen C, Umezawa Y, Kotov NV, Williams G, *et al.* A systems model for immune cell interactions unravels the mechanism of inflammation in human skin. *PLoS Comput. Biol.* 2010, 6(12):e1001024.

[35] Fantaye AK, Goshu MD, Zeleke BB, Gessesse AA, Endalew MF, *et al.* Mathematical model and stability analysis on the transmission dynamics of skin sores. *Epidemiol. infect.* 2022, 150:e207.

[36] Cross MC, Hohenberg PC. Pattern formation outside of equilibrium. *Rev. Mod. Phys.* 1993, 65(3):851.

[37] Turing AM. The chemical basis of morphogenesis. *Bull. Math. Biol.* 1990, 52(1):153–197.

[38] Harris MP, Williamson S, Fallon JF, Meinhardt H, Prum RO. Molecular evidence for an activator–inhibitor mechanism in development of embryonic feather branching. *Proc. Natl. Acad. Sci. U.S.A.* 2005, 102(33):11734–11739.

[39] Xu H, Sun M, Zhao X. Turing mechanism underlying a branching model for lung morphogenesis. *PloS one* 2017, 12(4):e0174946.

[40] Raspopovic J, Marcon L, Russo L, Sharpe J. Digit patterning is controlled by a Bmp-Sox9-Wnt Turing network modulated by morphogen gradients. *Science* 2014, 345(6196):566–570.

[41] Graham JH, Freeman DC, Emlen JM. Antisymmetry, directional asymmetry, and dynamic morphogenesis. In *Developmental Instability: Its Origins and Evolutionary Implications.* Dordrecht: Springer, 1994, pp. 123–139.

[42] Xu H, Sun M, Zhao X. Turing mechanism underlying a branching model for lung morphogenesis. *PLoS One* 2017, 12(4):e0174946.

[43] Gambino G, Lombardo M, Sammartino M. Pattern formation driven by cross-diffusion in a 2D domain. *Nonlinear Anal. Real World Appl.* 2013, 14(3):1755–1779.

[44] Lacitignola D, Bozzini B, Peipmann R, Sgura I. Cross-diffusion effects on a morphochemical model for electrodeposition. *Appl. Math. Modell.* 2018, 57:492–513.

[45] Diez A, Krause AL, Maini PK, Gaffney EA, Seirin-Lee S. Turing pattern formation in reaction-cross-diffusion systems with a bilayer geometry. *Bull. Math. Biol.* 2024, 86(2):13.

[46] Giunta V, Lombardo MC, Sammartino M. Pattern Formation and Transition to Chaos in a Chemotaxis Model of Acute Inflammation. *SIAM J. Appl. Dyn. Syst.* 2021, 20(4):1844–1881.

[47] De Kepper P, Castets V, Dulos E, Boissonade J. Turing-type chemical patterns in the chlorite-iodide-malonic acid reaction. *Physica D* 1991, 49(1–2):161–169.

[48] Astrov Y, Ammelt E, Teperick S, Purwins HG. Hexagon and stripe Turing structures in a gas discharge system. *Phys. Lett. A* 1996, 211(3):184–190.

[49] Spinelli L, Tissoni G, Brambilla M, Prati F, Lugiato L. Spatial solitons in semiconductor microcavities. *Phys. Rev. A* 1998, 58(3):2542.

[50] Short MB, Brantingham PJ, Bertozzi AL, Tita GE. Dissipation and displacement of hotspots in reaction-diffusion models of crime. *Proc. Natl. Acad. Sci. U.S.A.* 2010, 107(9):3961–3965.

[51] Tóth Á, Horváth D. Diffusion-driven instabilities by immobilizing the autocatalyst in ionic systems. *Chaos* 2015, 25(6):064304.

[52] Nesterenko AM, Kuznetsov MB, Korotkova DD, Zaraisky AG. Morphogene adsorption as a Turing instability regulator: Theoretical analysis and possible applications in multicellular embryonic systems. *PloS one* 2017, 12(2):e0171212.

[53] Kuznetsov M, Polezhaev A. Widening the criteria for emergence of Turing patterns. *Chaos* 2020, 30(3):033106.

[54] Younes GA, Kuznetsov M, Khatib NE, Volpert V. Mathematical modeling of the interaction of atherosclerotic inflammation and chemotaxis: formation of fatty streaks (Submitted).

[55] Penner K, Ermentrout B, Swigon D. Pattern formation in a model of acute inflammation. *SIAM J. Appl. Dyn. Syst.* 2012, 11(2):629–660.

[56] Nadin G, Ogier-Denis E, Toledo AI, Zaag H. A Turing mechanism in order to explain the patchy nature of Crohn's disease. *J. Math. Biol.* 2021, 83(2):12.

[57] Grudzinska MK, Kurzejamska E, Bojakowski K, Soin J, Lehmann MH, *et al.* Monocyte Chemoattractant Protein 1–Mediated Migration of Mesenchymal Stem Cells Is a Source of Intimal Hyperplasia. *Arterioscler. Thromb. Vasc. Biol.* 2013, 33(6):1271–1279.

[58] Gui T, Shimokado A, Sun Y, Akasaka T, Muragaki Y. Diverse roles of macrophages in atherosclerosis: from inflammatory biology to biomarker discovery. *Mediat. Inflamm.* 2012, 2012(1):693083.

[59] Ramji DP, Davies TS. Cytokines in atherosclerosis: Key players in all stages of disease and promising therapeutic targets. *Cytokine Growth Factor Rev.* 2015, 26(6):673–685.

[60] Almer G, Frascione D, Pali-Scholl I, Vonach C, Lukschal A, *et al.* Interleukin-10: an anti-inflammatory marker to target atherosclerotic lesions via PEGylated liposomes. *Mol. Pharmaceutics* 2013, 10(1):175–186.

[61] Oo YH, Shetty S, Adams DH. The role of chemokines in the recruitment of lymphocytes to the liver. *Digest. Dis.* 2010, 28(1):31–44.

[62] Mallat Z, Besnard S, Duriez M, Deleuze V, Emmanuel F, *et al.* Protective role of interleukin-10 in atherosclerosis. *Circ. Res.* 1999, 85(8):e17–e24.

[63] Haraux A. A simple characterization of positivity preserving semi-linear parabolic systems. *arXiv* 2016, arXiv:1610.09909.

[64] Williams JW, Giannarelli C, Rahman A, Randolph GJ, Kovacic JC. Macrophage biology, classification, and phenotype in cardiovascular disease: JACC macrophage in CVD series (part 1). *J. Am. Coll. Cardiol.* 2018, 72(18):2166–2180.

[65] Moro-García MA, Mayo JC, Sainz RM, Alonso-Arias R. Influence of inflammation in the process of T lymphocyte differentiation: Proliferative, metabolic, and oxidative changes. *Front. Immunol.* 2018, 9:339.

[66] Botelho F, Gaiko V. Global analysis of planar neural networks. *Nonlinear Anal-theor.* 2006, 64(5):1002–1011.

[67] Anderton H, Alqudah S. Cell death in skin function, inflammation, and disease. *Biochem. J.* 2022, 479(15):1621–1651.

[68] Nguyen AV, Soulika AM. The Dynamics of the Skin's Immune System. *Int. J. Mol. Sci.* 2019, 20(8):1811.

[69] Kuznetsov M, Kolobov A, Polezhaev A. Pattern formation in a reaction-diffusion system of Fitzhugh-Nagumo type before the onset of subcritical Turing bifurcation. *Phys. Rev. E* 2017, 95(5):052208.

[70] Kaminaga A, Vanag VK, Epstein IR. A reaction–diffusion memory device. *Angew. Chem. Int. Ed.* 2006, 45(19):3087–3089.

[71] Muratov C, Osipov V. Scenarios of domain pattern formation in a reaction-diffusion system. *Phys. Rev. E* 1996, 54(5):4860–4879.

[72] Van Gysel J, Grimalt R. A linear lesion in a child with atopic dermatitis: Not a coincidence. *Clin. Case Rep.* 2019, 7(9):1667–1669.

[73] Paulino L, Hamblin DJ, Osondu N, Amini R. Variants of erythema multiforme: A case report and literature review. *Cureus* 2018, 10(10):e3459.